RGNZ/MGPB

Mapping Rayleigh Wave Group Velocities from Ambient Noise in the Way Ratai Geothermal Field Using PiGraf Seismograph Prototypes

Rudarsko-geološko-naftni zbornik
(The Mining-Geology-Petroleum Engineering Bulletin)
UDC: 550:3
DOI: 10.17794/rgn.2025.2.1

Original scientific paper

Karyanto[1]*; Haidar Prida Mazzaluna[2]; I Gede Boy Darmawan[3]; Rahmat Catur Wibowo[4]; Ahmad Zaenudin[5]; Maman Hermana[6]

[1] Jl. Sumantri Brojonegoro, Bandar Lampung, Indonesia (Department of Geophysical Engineering, Faculty of Engineering, University of Lampung, 34145), ORCID 0000-0003-0189-4109

[2] Jl. Sumantri Brojonegoro, Bandar Lampung, Indonesia (Department of Geophysical Engineering, Faculty of Engineering, University of Lampung, 34145), ORCID 0009-0004-2203-5893

[3] Jl. Sumantri Brojonegoro, Bandar Lampung, Indonesia (Department of Geophysical Engineering, Faculty of Engineering, University of Lampung, 34145), ORCID 0000-0002-6368-4070

[4] Jl. Sumantri Brojonegoro, Bandar Lampung, Indonesia (Department of Geophysical Engineering, Faculty of Engineering, University of Lampung, 34145), ORCID 0000-0003-2754-1803

[5] Jl. Sumantri Brojonegoro, Bandar Lampung, Indonesia (Department of Geophysical Engineering, Faculty of Engineering, University of Lampung, 34145), ORCID 0000-0001-6458-8518

[6] Seri Iskandar, Perak Darul Ridzuan, Malaysia (Department of Geoscience, Faculty of Science and Information Technology, Universiti Teknologi PETRONAS, 32610), ORCID 0000-0002-0205-4446

Abstract

Since 2018, the research team has been investigating and developing a prototype sensor for recording seismic activity. An upgrade has been developed and must be evaluated, primarily to monitor ambient noise activities in the geothermal environment. This study aims to determine the group velocity of Rayleigh waves using ambient noise tomography (ANT) analysis in the Way Ratai geothermal region utilising four PiGraf seismograph prototypes. The acquisition method deploys a stationary inter-station around 5 kilometres (km) apart for seven consecutive days, with 100 samples per second (SPS). Fast marching surface tomography (FMST) has been utilised to generate group velocity from a cross-correlated time series, which produces tomographic images. The results showed that the ambient noise energy distribution originated from the northwest to the southeast, most likely from the sea. At the same time, the group velocity from the Green's function group in the period range 0.2 s to 0.5 s, 0.5 s to 1 s, and 1 s to 5 s are 0.337 km/s, 0.415 km/s, and 0.427 km/s, respectively. These values are aligned within the dispersion curve's velocity range of 0.3–0.8 km/s. The group velocity modelling of Rayleigh waves in the period range of 0.5 s to 1 s also identified a pattern corresponding with the geothermal potential area, confirming prior findings. However, the clarity of the cross-correlogram of the Green's function group was identified as a topic for further investigation, suggesting adding more stations and longer measurement times.

Keywords:
ambient noise tomography; geothermal; PiGraf prototype; Rayleigh wave group velocity; Way Ratai

1. Introduction

The Way Ratai geothermal field is a geothermal energy potential located on Mount Ratai, Pesawaran (**Karyanto, 2003; Karyanto et al., 2020**). However, there has been no significant improvement in the work status at Way Ratai. This condition certainly illustrates the slow development of geothermal power plants in Way Ratai. Academics can make efforts to increase investor confidence in the potential of geothermal resources in Way Ratai. Improved data analysis and modelling is one solution to increase the chances of success and reduce risks in well targeting to optimise drilling costs (**Abiyudo et al., 2021; Daud et al., 2017; Irfan and Daud, 2019**). Geothermal exploration efforts necessitate several data collection methods, one is microseismic recordings using the ambient noise tomography (ANT) methodology to describe subsurface structures in the geothermal region.

ANT has been utilised to discover information about subsurface features, basins, and upper crustal structures, including volcanic complexes (**Martha et al., 2017; Pranata et al., 2020; Rosalia et al., 2022; Zulfakriza et al., 2014, 2020**). Furthermore, the ANT approach has now become widely used for geothermal exploration activities (**Amoroso et al., 2018; Calò et al., 2013; Lehujeur et al., 2015; Martins et al., 2020; Sánchez-Pastor et al., 2021; Wahida et al., 2018**). The ANT approach

* Corresponding author: Karyanto
e-mail address: karyanto@eng.unila.ac.id

uses empirical Green's functions surface waves extracted from cross-correlated ambient noise waveforms obtained from pairs of seismic stations (**Sarjan et al., 2021**). **Bensen et al. (2007)** present an ANT processing approach that includes four primary stages: single data preparation, cross-correlation and stacking, group velocity measurements using the dispersion curve, and surface wave tomography.

ANT data acquisition is generally carried out using a network of seismograph stations. Each station has sensors, GPS, a power supply, and a data logger. The local scale network of ANT metering stations is generally temporary, although some stations are permanent (**Lehujeur et al., 2017; Martha et al., 2017; Sarjan et al., 2021**). Several types of seismograph instruments used in microseismic measurements include Trillium, Lennartz, Guralp, Far Field Nodal, Geobit, BBVS, CMG-3T, STS-2, L4C, and others. These instruments consist of short-period and broadband seismographs (**Sarjan et al., 2021**). The need for this instrument prompted the research team to develop a seismograph by utilising the accelerometer instrument that had been previously developed (**Darmawan et al., 2021; Karyanto et al., 2022**). The upgrade is done by replacing the accelerometer sensor with a geophone. The increase in bandwidth is also achieved by upgrading the Analogue to Digital Converter (ADC) module to 24-bit.

This study aims to investigate the seismograph prototype response in detecting the area of geothermal fluid activity connected with geological formations via the ANT approach. The data is processed using the cross-correlation method until the dispersion extract is utilised for tomographic inversion, yielding a group velocity map. Group velocity maps are used to identify subsurface characteristics, such as fluid circulation zones or porous structures. As a result, in 2018, the research team created a prototype upgrade from an accelerometer (**Karyanto et al., 2022**) to a seismograph termed PiGraf. This upgrade is necessary to capture lower-frequency seismic waves using 4.5 Hz geophone sensors. In addition, the ADC system upgrade from 16-bit to 24-bit was also carried out to overcome the weaknesses of the previous prototype (Akselino v1) which was not yet able to properly record frequencies below 1 Hz (**Amiruddin et al., 2020; Darmawan et al., 2021**) and Akselino v2 is only able to characterise near-surface features based on shallow shear wave velocities (**Karyanto et al., 2022, 2024b**). With the addition of a 24-bit ADC and a minimum of 100 samples per second (SPS), it is hoped that this PiGraf seismograph prototype will be able to increase sensitivity and signal-to-noise ratio, especially in recording ambient noise so that it can be used in identifying deeper structures, especially in geothermal fields.

2. Methods and material

Four seismograph prototypes (PiGraf) were installed on fixed measuring stations for seven days in a row. The station is located surrounding the Way Ratai geothermal reservoir potential site, with one station near the manifestation site for an interstation distance of 5 km on average. This arrangement is based on previous studies identifying the reservoir potential in Way Ratai around 9 km with a depth of 0.5 - 1.5 km (**Karyanto et al., 2021; Karyanto et al., 2024a**). In addition, the distance between these stations also considers several seismograph station models used in other studies for ANT measurements in geothermal environments (**Gaucher et al., 2019; Granados-Chavarría et al., 2022; Lehujeur et al., 2017; Matzel et al., 2017; Muksin et al., 2013; Nayak et al., 2018; Patlan et al., 2013; Zhou et al., 2021**). PiGraf is a seismograph prototype developed by a research team (**Amiruddin et al., 2020; Darmawan et al., 2021**). The development of PiGraf has successfully passed several stages of laboratory and field testing with the REFTEK Accelerograph as a comparative instrument (**Karyanto et al., 2022**). The results indicated a considerable improvement in the sensitivity and data logging system. Previous test results demonstrated the viability of constructing a 24-bit data system with a 4.5 Hz geophone sensor. Based on this change's results, tests were conducted in the Way Ratai geothermal field (**Karyanto et al., 2024b**). Before data acquisition in the field, the PiGraf prototype successfully validated the suitability of time and the first break in an array with the comparative seismograph GAMADU Seismometer (formerly known as AMADU) (**Meilinda et al., 2023**). The seismograph prototype (PiGraf) has been erected at an acquisition station with three axes: one vertical and two horizontals oriented north-south and west-east, respectively. All four stations share a single time parameter based on the GPS time associated with each seismograph. The acquisition mode is recorded continuously for 24 hours daily at a sample rate of 100 SPS. Daily seismograph battery replacement and data download were conducted to avoid battery power depletion or loss.

2.1. Geological condition

The geological properties of Way Ratai and the presence of geothermal manifestations influence the selection of the station location (see **Figure 1**). Geologically, the PG03 station is placed on the Quarternary Volcanic Lava rock formation (in the geological map given the symbol Qhv) close to the Mount Ratai peak (**Mangga et al., 1993**). Ambient noise measurements at this location approach the heat source zone estimated to be below the summit of Mount Ratai (**Karyanto et al., 2021**). Meanwhile, the PG01 station is located adjacent to the manifestation area. It is in the Tertiary Period of the Hulusimpang Formation (Tomh), composed of andesite-basalt lava rocks, tuff, and volcanic breccia (**Mangga et al., 1993**). This formation is considered where the Way Ratai geothermal reservoir is located (**Karyanto et al., 2021**). The formation also has a relatively thick layer of altered clay identified as caprock (**Karyanto et al., 2024a**). The

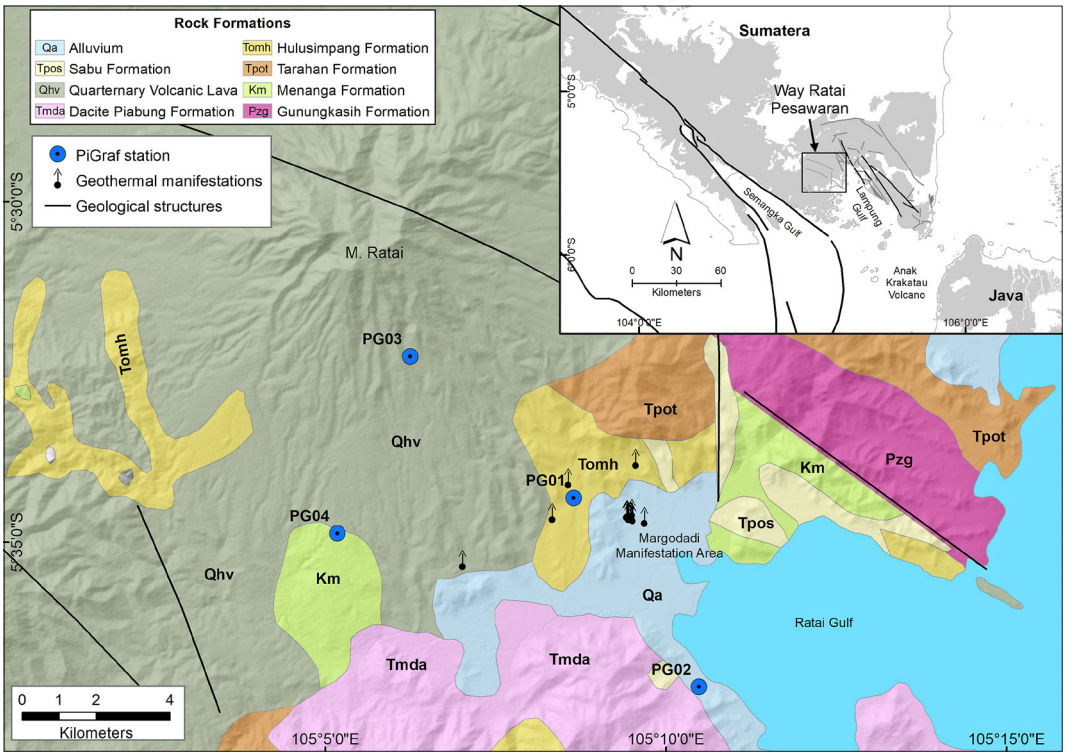

Figure 1: Location of PiGraf station for ANT measurement on the regional geological map of the research area

next station is placed in another formation, namely PG04, in the Cretaceous Period of Menanga Formation (Km), consisting of shale and clay rocks with reed and limestone inserts (**Mangga et al., 1993**). Meanwhile, station PG02 is placed at the southernmost point and closest to the sea during the Holocene Epoch of Alluvium Formation (Qa).

The Way Ratai geothermal region is distinguished by volcanic activity and structural characteristics that enhance its geothermal potential. The region consists of volcanic units, including lava domes, flows, and pyroclastic products, which erupted throughout the Pleistocene to Holocene (**Al-Hassan and Iqbal, 2022**). The region's structural lineaments, notably the Lampung-Panjang Fault, follow northwest-southeast and northeast-southwest tendencies (**Sulandari et al., 2023**). These structures impact geothermal manifestations and seismic activity in the surrounding environment. Lampung's geology is complicated, with sedimentary formations like the Sabu Formation coming from the collision between the Woyla volcanic arc and the West Sumatra Plate during the Paleogene (**Widiatama et al., 2022**). Geophysical studies, particularly gravity techniques, have explored the region's underlying structure and geothermal potential (**Sarkowi et al., 2021; Taufiq, 2020**). The area has northwest-southeast and southwest-northeast trending fault structures compatible with the significant regional fault patterns. Similar structural tendencies have been seen in the neighbouring Natar geothermal area, implying a link with the Great Sumatran Fault system (**Juliarka and Iqbal, 2020**). These findings highlight intriguing geothermal opportunities in the Way Ratai region, which merit additional research and development.

2.2. Ambient Noise Cross-correlation

Ambient noise employs the technique of seismic interferometry between two signals to investigate their propagation medium (**Cankurtaranlar and Demirbağ, 2023; Verdel et al., 2019**). Ambient noise tomography (ANT) uses the cross-correlation of two seismic signals to create an impulse response between them (**Rosalia et al., 2020; X. Yang et al., 2023**). The cross-correlation of two signals produces Green's function for the medium through which the wave propagates. Green's function is the reaction of the wave propagation medium to the source impulse (**Barmin et al., 2011; Denolle et al., 2014; Viens et al., 2016**). In general, ANT is a time-based correlation of signals captured simultaneously at two stations, leading to an impulse response between them. Consequently, one station functions as the source and the other as the receiver, assuming the adjacent station has sufficient ambient noise sources. In such a situation, the cross-correlation between the two stations will be able to construct Green's function (**Ikeda et al., 2021; Larose et al., 2015; Wang et al., 2019**). Preparing data is required before cross-correlation, especially if the raw data would emphasise ambient noise. This method eliminates undesirable signals, such as instrument aberrations and earthquakes, which can mask ambient noise data (**da Silva et al., 2021**). The stages of this process include data sampling reduction, instrument correction, data detrend and demean, temporal normalisation, and

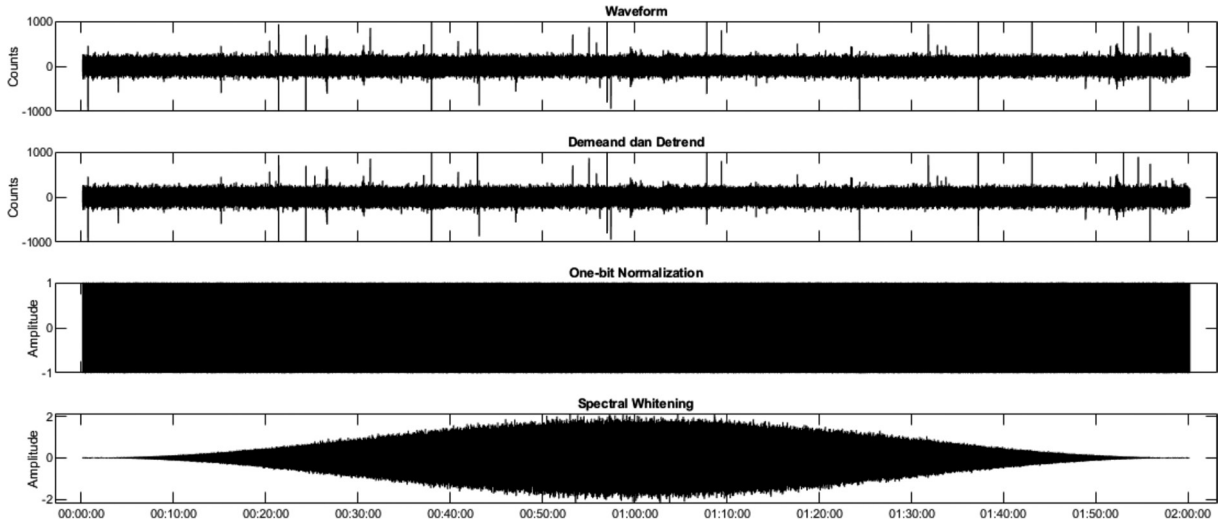

Figure 2: Snapshot of data preprocessing per 2 hours at PG02 station

frequency whitening (**Anshori et al., 2018; Bensen et al., 2007**).

Preprocessing in the current study has been carried out in multiple stages, including sampling rate reduction, instrument correction, detrend and demean data, one-bit normalisation, frequency bleaching, and bandpass filtering (see **Figure 2**). However, no instrument adjustment was performed in this case because the utilised tool was the same sort of seismometer. The entire preprocessing process has been carried out using the Ambient Noise Cross-correlation for Daily Long program by **Yao (2015)**. The selection of the maximum period in the period range is given by **Bensen et al. (2007)**, where the distance between stations (Δ) is at least 2–3 times the wavelength (λ). **Equations 1-3** approximate the Rayleigh wave group velocity (U) (**Bensen et al. 2007**).

$$U = \lambda / \mathrm{T} \tag{1}$$

$$\Delta_{\min} = 2\lambda \tag{2}$$

$$T_{\max} = \Delta / 2\mathrm{U} \tag{3}$$

where T is the period, and the maximum period equation (T_{max}) is obtained in **Equation 3**.

In the process of preprocessing ambient noise data, it is necessary to resample the data to save processing time. Generally, the new frequency is 1 Hz (**Seichter et al., 2017; Xia et al., 2023**). However, the new data sampling method is 5 Hz, which is appropriate given that the data processed is just seven days long. Then, using **Martha et al.'s (2017)** processing scheme, the data segment for cross-correlation is two hours. The data output to be obtained is a cross-correlation function. The processed cross-correlation data can display the data group of cross-correlation functions on the correlogram. The cross-correlation is calculated using **Equation 4** (**Liu et al., 2018**).

$$C_{12}(t) \approx \int_0^{t_n} v_1(\tau)\, v_2(t+\tau)\, d\tau \tag{4}$$

where $C_{12}(t)$ is a function of ambient noise cross-correlation in the time domain, $v_1(t)$ and $v_2(t)$ is broadband data that has been preprocessed at stations 1 and 2. While t and t_n is a time lag between $v_1(t)$ and $v_2(t)$ and the length of the data used for cross-correlation, respectively.

Green's function in the time domain can be calculated by taking the derivative of the noise cross-correlation's time function. For station pairs 1 and 2, the relationship between the ambient noise cross-correlation, the empirical Green's function, and the original Green's function are shown using **Equation 5** (**Liu et al., 2018**).

$$\frac{dC_{12}(t)}{dt} = -\hat{G}_{12}(t) + \hat{G}_{21}(t) \approx -G_{12}(t) + G_{21}(t) \tag{5}$$

where $dC_{12}(t))/dt$ is the first derivative of the cross-correlation of ambient noise in the time domain $dC_{12}(t))$, while $\hat{G}(t)$ and $G(t)$ are the empirical and the original Green's function, respectively.

2.3. Energy distribution and dispersion curve

The primary source of ambient noise is ocean gravity waves, especially ocean waves with a frequency range below 1 Hz (**Li et al., 2022; Nishida, 2017**). The amplitude of ambient noise is also generally higher in coastal areas than in continental areas (**Nishida, 2017**). In a study conducted in Japan, Rayleigh waves from secondary microseisms were sensitive to local ocean wave activity, showing seasonal directional variations correlated with the source region of ocean stress. This directional bias can cause variations in the recorded seismic signal, depending on its proximity to the coastline (**Nishida et al., 2024; Takagi et al., 2018**). In addition, the depth and homogeneous distribution of sources play a role in recovering surface waves (**Halliday and Curtis, 2008**).

This study employs **Yao and van der Hilst's (2009)** plane wave modelling technique to disperse ambient noise energy by calculating the average amplitude of a collection of cross-correlation functions in the signal window at each azimuth angle interval. To get the final cross-correlation function, sum the cross-correlation functions for all waves with azimuth angles ranging from 0 to 2π. The relationship between the cross-correlation functions of $C_{12}(\omega,t)$ with ambient noise energy is given in **Equation 6** (**Yao and van der Hilst, 2009**).

$$C_{12}(\omega,t)=\int_0^{2\pi} E_p(\omega,\theta)\cos\left[\omega(t-\delta t)\right]H(t,\delta t)\,d\theta \quad (6)$$

where E_p is an ambient noise energy, and $H(t,\delta t)$ is a taper function. Then, a pie chart showing the azimuthal direction of ambient noise is obtained. It shows where the direction of ambient noise comes from by looking at the highest normalised amplitude (**Takagi et al., 2018**).

The next stage of processing the Rayleigh wave velocity dispersion curve is carried out using the Dispersion Analysis Matlab GUI software by **Yao (2015)**. The required data input is a station list file, a waveform file in the form of a cross-correlation function, or an empirical Green's function. The setup parameters are the width of the dispersion curve window, including the velocity range (km/s) and the period range (s), the period range value for the filter in the time domain, selecting the group velocity or phase velocity to be selected to be captured and stored, the data to be processed, and the selection of the Rayleigh wave velocity or Love wave velocity (**Yao, 2015; Yao et al., 2006, 2008, 2011**). Afterwards, the dispersion curve obtained can be picked to get the velocity value for each period.

Meanwhile, ambient noise tomography was carried out by making a Rayleigh wave velocity map using the fmst v1.1 program by **Rawlinson (2005)**. In this program, inversion is carried out by inverting the time of waves between stations for each period. In carrying out this inversion, the Fast-Marching Method (FMM) approach tracks the wavefront on a heterogeneous medium (**Rawlinson et al., 2006; Rawlinson and Sambridge, 2005**). The assumption that the inversion step is linear makes this technique non-linear. However, the repetitive use of FMM enables a non-linear connection between velocity and travel time (**Saygin and Kennett, 2012**). The line connecting the two stations is continually updated during iterative inversion. FMM employs a grid-based numerical technique that propagates from a point to a parallel direction as much as feasible (**Amiri et al., 2023; Dahiya and Baskar, 2015; Rawlinson and Sambridge, 2004; Xu et al., 2023**). FMM is used to perform travel time calculations and raypath direction tracking (**Guan and Niu, 2018; Wu et al., 2022**). Using two methods, most numerical approaches consider travel time and beam direction (**Fang et al., 2015; van Hal et al., 2023**). The first method is to solve the ray kinetic equation using the ray-based method. The second technique is to solve the eikonal equation or calculate the time travelled by the surface wave gradient to identify the quickest path between two places (**Ritzwoller et al., 2011; White et al., 2020**).

3. Results and discussion

The average Rayleigh wave group velocity is often calculated by plotting the group of green functions from one station to another in a cross-correlogram (see **Figure 3**), where the arrival time of the waves is proportional to the distance between stations. As a result, the average Rayleigh wave group velocity may be calculated using the high amplitude provided by the group of Green's functions. However, in this study, it is not easy to discern the link between the distance and the arrival duration of the Rayleigh wave since the resultant Green's function does not accurately predict the Rayleigh wave's position. Nevertheless, the average velocity can still be seen by looking at the continuous high amplitude contained in the Green's function group. The group of Green's functions used to pick up signals has a travel time of up to 40 seconds and a distance between stations of up to 14 km, considering that the farthest distance between stations is about 12 km. The velocity window of the Rayleigh wave group utilised is 0.2–1 km/s, as illustrated by the red dotted line in **Figure 3**. The gradient of the continuous line revealed that the average group velocity was 0.337 km/s for the period of 0.2–0.5 seconds, 0.415 km/s for the period of 0.5–1 second, and 0.427 km/s for 1–5 seconds.

Based on the dispersion curve (see **Figure 3**), it is clear that there is a waveform gap at a distance between stations of less than 5 km and a distance of 7–10 km. This gap is caused by the absence of measurement stations at that distance. Optimal seismograph network geometry can increase resolution and minimise uncertainty in seismic parameter estimates (**Rabinowitz and Steinberg, 2000; Uhrhammer, 1980**). So, adding seismograph stations will increase spatial resolution and data quality, thereby increasing the clarity of the cross-correlogram. Adding at least two to four additional stations also supports the results of previous studies, which state that it can significantly increase data clarity (**Halim et al., 2022; Trnkoczy et al., 2009**). In addition, other factors, such as environmental influences including wind and sea waves, can affect noise measurements (**Lynch et al., 1993**). In this study, the influence of rainy weather and human activities also affected the recording quality. However, several techniques have been developed to reduce these effects and improve the signal-to-noise ratio (**Tian and Ritzwoller, 2017**), one of which is by using long-duration recordings (e.g. 1 year) that can amplify strong ambient noise coming from most directions and ensure the accuracy of the empirical Green's function and ambient noise tomography (**Yang and Ritzwoller, 2008**).

This investigation uses the azimuth angle interval of 20 degrees and cross-correlation function in the range of

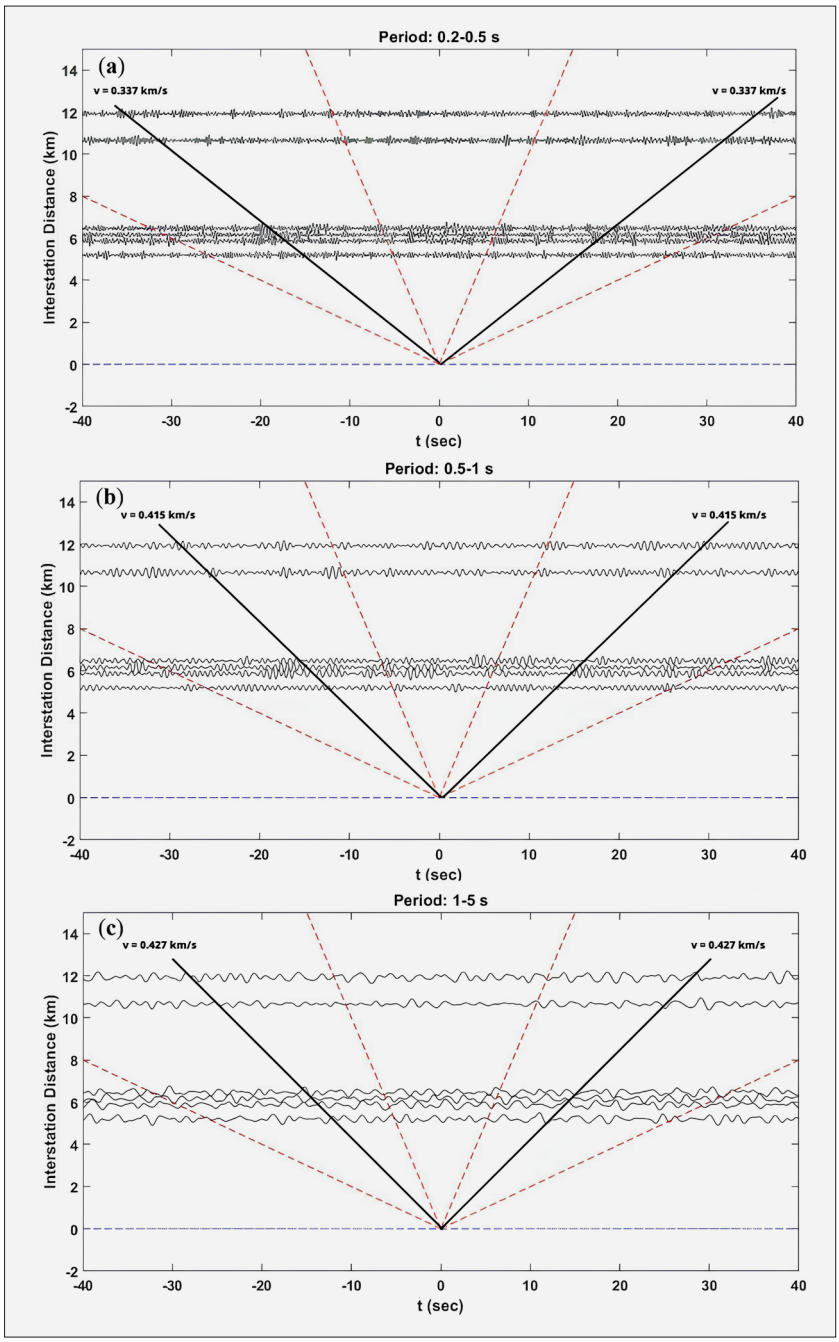

Figure 3: Bandpass filtered components of Green's functions at 0.2– 0.5 s (a), 0.5– 1 s (b), and 1– 5 s (c).

0.2–0.5 seconds, 0.5–1 second, and 1–5 seconds (see **Figure 4**). As a result, the energy distribution has a value range of 0–1, where the higher value indicates that more ambient noise is recorded from the azimuth angle. The predominant direction of the source of ambient noise in the research area is northwest-southeast, namely at the azimuth of 110º–150º and 290º–330º. Those three different period ranges obtained similar results, namely the dominant ambient noise energy source in the northwest-southeast direction. In the research area, the west-southeast direction is ambient noise from the sea direction, namely Ratai Gulf, which is also part of Lampung Bay (see **Figure 1**). This source of ambient noise is most dominant in 1–5 seconds. It is in line with previous research, which states that the primary source of ambient noise is the interaction of ocean waves with the land (**Yao and van der Hilst, 2009**).

3.1. Group velocity of dispersion curve

The Green's function can be analysed further by obtaining a dispersion curve. Analysis of the dispersion curve results in a function of the velocity of each wave period. In this study, the dispersion curve was carried out to obtain the group velocity per wave period on each station pair (see **Figure 5**). The wave period taken is from 0.2 seconds to the maximum period of the station pair cross-correlation function. This maximum period is calculated using **Equation 3**. The vertical red line in some

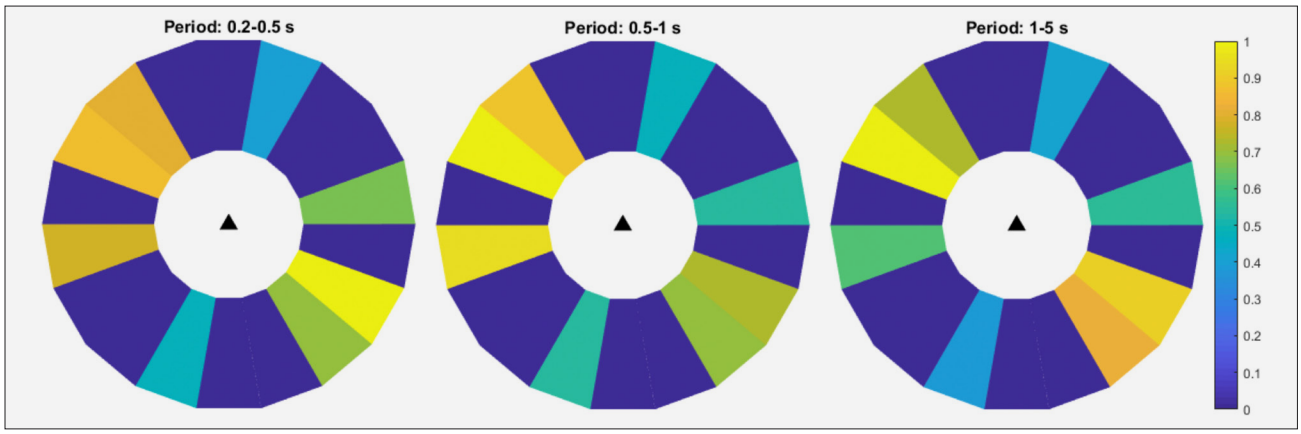

Figure 4: Ambient noise energy distribution of each period

of the dispersion curve images is the maximum period of the limit for picking group velocity. The dispersion curve of almost all station pairs is relatively poor, wherefore the input of Green's function is also inadequate in terms of quality. The station pairs considered passable at displaying the dispersion curve are the PG01-PG02, PG01-PG03, and PG03-PG04.

To calculate the signal-to-noise ratio (SNR), divide the signal window's high amplitude by the noise window's average amplitude. A blue waveform indicates the signal window, and a red waveform indicates the noise window (SNR) as a data-picking parameter. The trend of SNR decreases with the increase in periods. The separation across stations influences SNR trends. The more significant the gap between the separating stations, the longer the period might be. Therefore, SNR in pairs of stations with a longer distance, such as PG02-PG03 and PG02-PG04, has higher values. This result follows **Fichtner's (2015)** opinion regarding source-structure exchange due to decreased sensitivity with increasing distance from the receiver. However, these two stations do not have an excellent continuous dispersion curve. The picking velocity values are plotted into scatter plots to compare the velocity per period in each station pair, as shown in **Figure 6**. The inter-station velocity dispersion curve PG03-PG04 has the lowest velocity. In contrast, the interstation group velocity PG01-PG03 is the fastest. The velocity range for the dispersion curve is 0.3 - 0.8 km/s. These results reflect differences in the lithological conditions of rocks and subsurface characteristics passed by seismic waves, including the possibility of geothermal reservoirs at low surface wave velocities (**Wahida et al., 2018**).

3.2. Rayleigh wave group velocity map

The velocity of the Rayleigh wave group is obtained through repeated iterations. The input needed is the travel time between stations in a period of 1 second, which can be obtained from Green's function and the dispersion curve. The initial model uses a velocity of 0.415 km/s taken from the average group velocity in 0.5 – 1 second, with a grid dimension of 7×10 and a grid spacing of 2 km. The grid dimensions and spacing are adjusted to the desired number of raypaths and resolutions. In this study, because it is still in the experimental stage of the PiGraf prototype, only six raypaths can be used. Hence, the grid has been adjusted to skip the existing raypath. Modelling iterations were carried out seven times with a Root Meas Square (RMS) value of 0.38 s and a data variation of 0.14 s. This value is considered sufficient, considering the decline in RMS value in iterations is not too significant. The Rayleigh wave group velocity map modelled is shown in **Figure 7**.

The dominant velocity on the map (see **Figure 7**) is the average velocity in the initial model. Low-velocity patterns appear near geothermal manifestations and on the slopes of Mount Ratai, which is in line with previous research and has the potential to be the location of geothermal reservoirs (**Haerudin et al., 2016; Karyanto et al., 2020, 2021; Karyanto et al., 2024a; Suryadi et al., 2017**). These results also align with previous research that shows that geothermal reservoirs have low-velocity anomalies compared to their surrounding areas. It is because rocks in geothermal reservoirs generally have natural fractures (**Sánchez-Pastor et al., 2021**) and contain water as a critical aspect of sustainability (**Utama et al., 2024**). In addition, seismic velocity is directly proportional to density and inversely proportional to temperature (**Ali et al., 2023; Roth et al., 2000**). These results support previous studies that in geothermal environments, low-velocity ranges (typically less than 0.6 km/s) are often associated with geothermal reservoir potential (**Janssen et al., 2021; Tavip Dwikorianto et al., 2023; Wahida et al., 2018**). While higher velocity ranges can indicate dense magma chambers or dense rock formations. In geothermal systems, these high-velocity areas can represent cap rocks containing geothermal fluids beneath, effectively sealing the reservoir (**Janssen et al., 2021; Wahida et al., 2018**). Seismic velocity variations can also indicate transitions between rock types or structural features, such as volcanic systems influencing geothermal activity (**Fukushima et al.,**

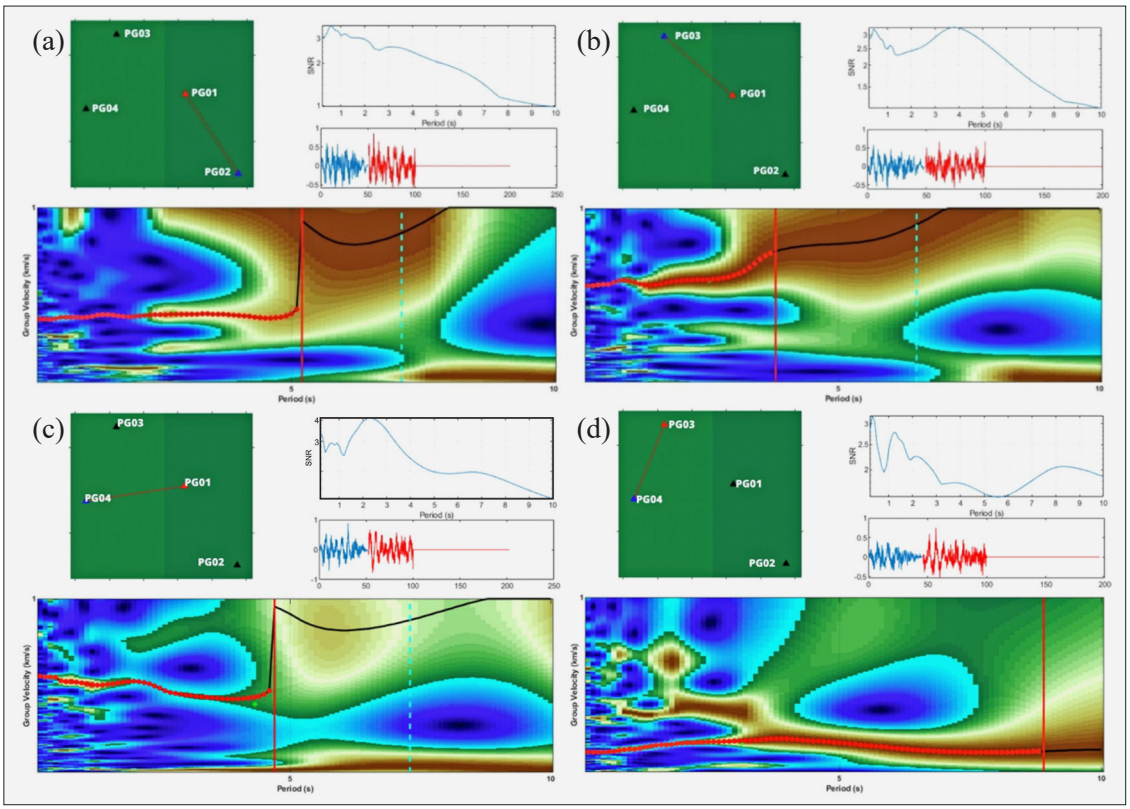

Figure 5: Dispersion curves of station pairs PG01-PG02 (a), PG01-PG03 (b), PG01-PG04 (c), and PG03-PG04 (d)

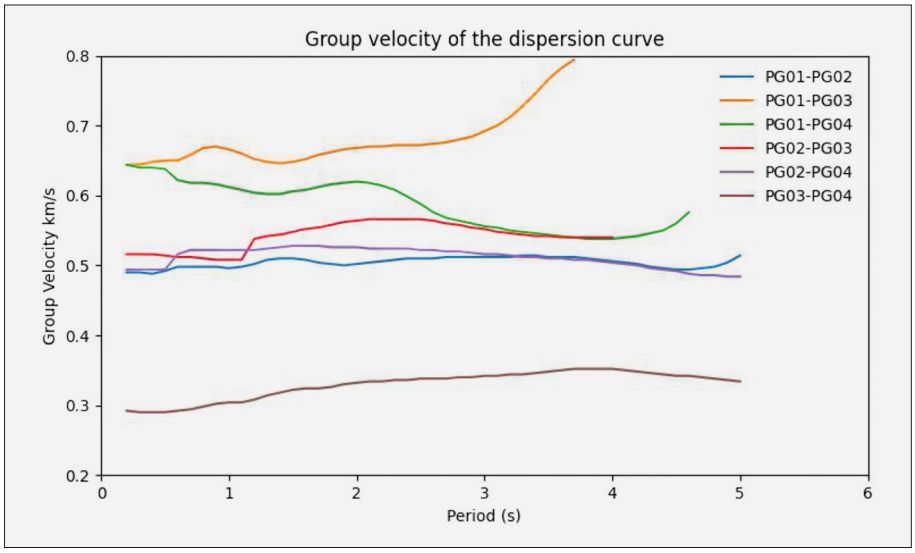

Figure 6: Group velocity of modelling results on dispersion curves

2024; Tryggvason et al., 2002). Thus, in this study, the low-velocity area of less than 0.6 km/s shown in **Figure 7** can be associated with the geothermal reservoir zone and is positively correlated with previous studies, which found that the reservoir zone is on the slopes of Mount Ratai (**Karyanto et al., 2021**). In addition, the area near the manifestation with low velocity is also in line with the thick alteration clay layer from previous studies (**Haerudin et al., 2016; Karyanto et al., 2024b**). This thick clay layer is considered to affect the characteristics of the spectral response period and peak ground acceleration (PGA) (**Li and Li, 2023**).

The Rayleigh wave group velocity map from ANT is arguably underrepresented due to the limited number of raypaths, especially for areas outside the raypath. In contrast, the velocity expansion beyond the raypath is the grid bearing required by the program. The FSMT algorithm is vital in generating group velocity maps that provide detailed insight into how different frequencies travel through different geological layers beneath the

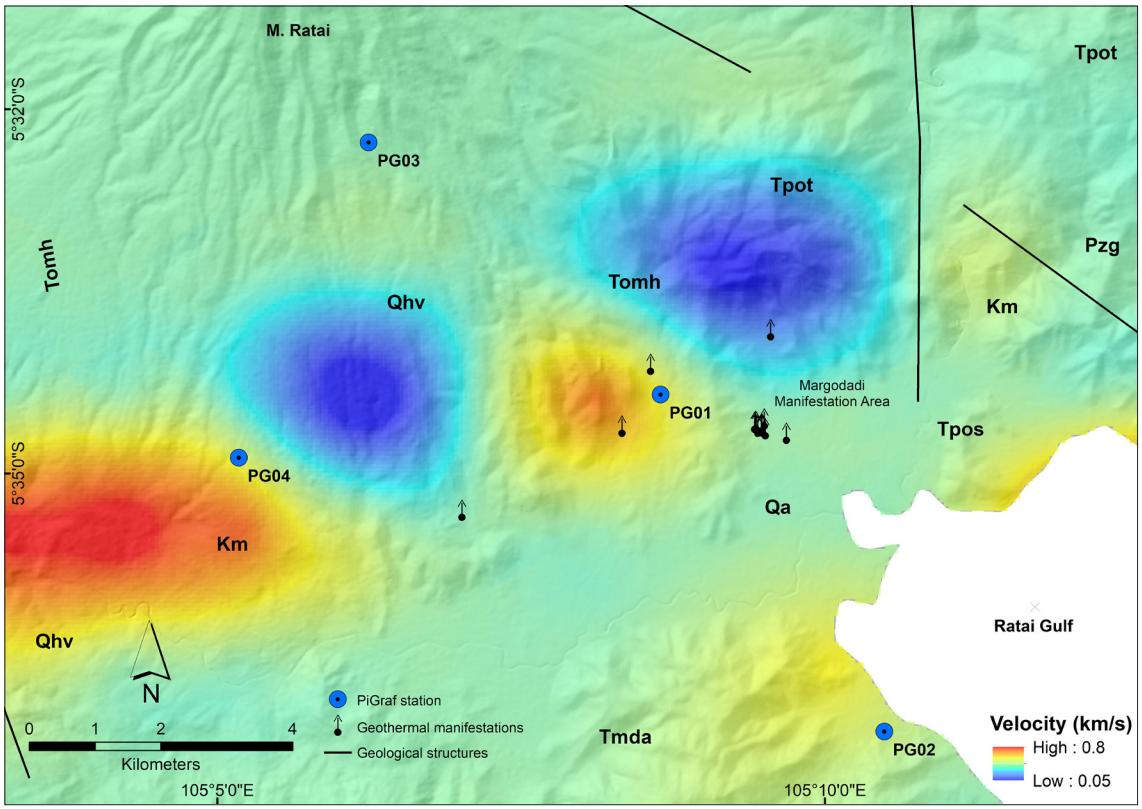

Figure 7: Rayleigh wave group velocity map with ANT 0.5 – 1 second

surface (**Amiri et al., 2023; Paulatto et al., 2022**). However, this method cannot overcome the decreasing trend of Signal to Noise Ratio (SNR) at increasing station distances. In contrast, this method can perform anomalous solid contrasts in areas with good track coverage. Therefore, further research can consider other alternative methods, such as surface wave eikonal tomography, which offers advantages in heterogeneous media and requires less a priori information, although they require accurate phase arrival time measurements and sufficient source coverage (**Dahiya and Baskar, 2015; Gouédard et al., 2012; Guan and Niu, 2018; White et al., 2020**). Nevertheless, considering that this study is the initial stage of directly testing the PiGraf prototype in the field, it can be said that these results are adequate. PiGraf can identify ambient noise energy sources in a period range of 0.2–5 seconds and produce a dispersion curve and velocity map of the Rayleigh wave group that conforms with the geothermal potential area of the previous study (**Karyanto et al., 2021; Karyanto et al., 2024a; Karyanto et al., 2024b**).

5. Conclusions

In order to study the response of the PiGraf seismograph prototype in a geothermal environment, we performed microseismic data acquisition and processing using the ANT method. With the enhancement of the 4.5 Hz geophone sensor and 24-bit ADC system, this prototype successfully performed acquisition with 100 SPS for 7 days spread across 4 measurement stations. The resulting data were then processed using the ambient noise cross-correlation technique to produce a velocity set based on Green's function with a period of 0.2 s to 5 s. Dispersion curve analysis was also performed to obtain a Rayleigh wave velocity map with the same period range.

This study identified the source of ambient noise from the northwest-southeast ocean. This study also obtained the average wave velocity from the Green's function set, namely 0.377 km/s in the period 0.2 to 0.5 s, 0.415 km/s in the period 0.5 to 1 s, and 0.427 km/s in the period 1 to 5 s. Meanwhile, the Rayleigh wave velocity group map ranging from 0.3 to 0.8 km/s also identified the potential reservoir zone and geothermal geological features on the slopes of Mount Ratai and around the manifestation. This finding also aligns with several previous research results related to the geothermal potential zone in Way Ratai, including the presence of a thick clay caprock layer on the low-velocity map.

Despite these successes, this study also managed to identify several weaknesses and constraints, such as unclear Green's function velocity curves and a decrease in signal-to-noise ratio at further station distances. The presence of waveform gaps at station distances of less than 5 km and distances between 7-10 km is suspected to cause the unclear amplitude of the velocity curve dispersion. In addition, environmental disturbances such as weather and human activities near the station can worsen data quality. Therefore, we suggest adding the num-

ber of measurement stations to overcome waveform gaps and measuring time to increase the number of stackings in order to increase the resolution of Green's function velocity dispersion curve and Rayleigh wave velocity. Furthermore, from these results, it can be concluded that the PiGraf prototype can record microseismic waves quite well, including ambient noise at lower frequencies, so it has the opportunity to continue to be developed, especially related to its sensitivity and validation tests.

Acknowledgement

Thanks to the geophysical instrumentation laboratory for allowing laboratory equipment, thanks to **Rawlinson (2005)** and **Yao (2015)** for the script code. Thanks also to Mr. Aceng and Mr. Darno, who helped with the acquisition activities at Way Ratai.

This research was supported by a collaborative partnership between the University of Lampung (No: 2985/UN26.21/PN/2023) and the Universiti Teknologi PETRONAS (UTP) (No: 015ME0-357).

6. References

Abiyudo, R., Daud, Y., and Satya, D. Y. (2021): Subsurface Structure Identification from Gravity Modelling of Silangkitang Geothermal Field for Future Injection Well Targeting. *Proceeding Digital Indonesia International Geothermal Convention (DIIGC)*, *2*,1-7.

Al-Hassan, M. A., and Iqbal, M. (2022): Volcanostratigraphy Study of Way Ratai Geothermal Prospect in Pesawaran Regency, Lampung Province. *IOP Conference Series: Earth and Environmental Science*, *1014*(1). https://doi.org/10.1088/1755-1315/1014/1/012005

Ali, A., Haq, S. U., Ali Shah, S. I., Khan, I., Aljohani, A. S., Jan, S. U., and Andualem, M. (2023): Heat Transfer Analysis of Generalised Nanofluid with MHD and Ramped Wall Temperature Using Caputo–Fabrizio Derivative Approach. *Mathematical Problems in Engineering*, *2023,* 8834891. https://doi.org/10.1155/2023/8834891

Amiri, S., Maggi, A., Tatar, M., Zigone, D., and Zaroli, C. (2023): Rayleigh wave group velocities in North-West Iran: SOLA Backus-Gilbert vs. Fast Marching tomographic methods. *Seismica*, *2*(2). https://doi.org/10.26443/seismica.v2i2.1011

Amiruddin, A., Suharno, S., and Karyanto, K. (2020): Desain Dan Realisasi Accelerometer Berbasis Arduino Sebagai Instrumen Pendeteksi Mikrotremor. *Jurnal Geofisika Eksplorasi*, *5*(3), 3–14. https://doi.org/10.23960/jge.v5i3.31

Amoroso, O., Festa, G., Bruno, P. P., D'Auria, L., De Landro, G., Di Fiore, V., Gammaldi, S., Maraio, S., Pilz, M., Roux, P., Russo, G., Serlenga, V., Serra, M., Woith, H., and Zollo, A. (2018): Integrated tomographic methods for seismic imaging and monitoring of volcanic caldera structures and geothermal areas. *Journal of Applied Geophysics*, *156,* 16–30. https://doi.org/10.1016/j.jappgeo.2017.11.012

Anshori, M., Maryanto, S., Rahman, T. D., and Panshori, A. (2018): Ambient Noise Tomography for Determining the Velocity Model of Rayleigh Wave in Java Island, Indonesia. *International Journal of Applied Physics*, *5*(1), 9–13. https://doi.org/10.14445/23500301/IJAP-V5I1P103

Barmin, M. P., Levshin, A. L., Yang, Y., and Ritzwoller, M. H. (2011): Epicentral location based on Rayleigh wave Empirical Green's Functions from ambient seismic noise. *Geophysical Journal International*, *184*(2), 869–884. https://doi.org/10.1111/j.1365-246X.2010.04879.x

Bensen, G. D., Ritzwoller, M. H., Barmin, M. P., Levshin, A. L., Lin, F., Moschetti, M. P., Shapiro, N. M., and Yang, Y. (2007): Processing seismic ambient noise data to obtain reliable broadband surface wave dispersion measurements. *Geophysical Journal International*, *169*(3), 1239–1260. https://doi.org/10.1111/j.1365-246X.2007.03374.x

Calò, M., Kinnaert, X., and Dorbath, C. (2013): Procedure to construct three-dimensional models of geothermal areas using seismic noise cross-correlations: Application to the soultz-sous-forêts enhanced geothermal site. *Geophysical Journal International*, *194*(3), 1893–1899. https://doi.org/10.1093/gji/ggt205

Cankurtaranlar, A., and Demirbağ, E. (2023): Utilisation of ambient noise seismic interferometry to retrieve P-wave reflections at Soma coal basin, Western Turkey. *Geophysical Prospecting*, *71*(7), 1356–1367. https://doi.org/10.1111/1365-2478.13403

da Silva, C. C., Poveda, E., da Silva Dantas, R. R., and Julià, J. (2021): Ambient Noise Tomography with Short-Period Stations: Case Study in the Borborema Province. *Pure and Applied Geophysics*, *178*(5), 1709–1730. https://doi.org/10.1007/s00024-021-02718-x

Dahiya, D., and Baskar, S. (2015): Characteristic fast marching method on triangular grids for the generalised eikonal equation in moving media. *Wave Motion*, *59*, 81–93. https://doi.org/10.1016/j.wavemoti.2015.07.007

Darmawan, I. G. B., Mulyasari, R., and Amukti, R. (2021): Perbandingan Indeks Kerentanan Seismik Antara Instrumen Akselerometer ADXL345 Dengan REFTEK 130-SMHR Menggunakan MetodeHorizontal-to-Vertical Spectral Ratio. *Jurnal Geofisika*, *19*(1), 10–16.

Daud, Y., Darma, S., Nuqramadha, W. A., Pratama, S. A., and Fahmi, F. (2017): Applying Innovations in MT Technology For Reducing Geothermal Exploration Risks. *Proceedings 39th New Zealand Geothermal Workshop*, 1–9.

Denolle, M. A., Miyake, H., Nakagawa, S., Hirata, N., and Beroza, G. C. (2014): Long-period seismic amplification in the Kanto Basin from the ambient seismic field. *Geophysical Research Letters*, *41*(7), 2319–2325. https://doi.org/10.1002/2014GL059425

Tavip Dwikorianto, Daud, Y., Agustya Adi Martha, and Aditya A Juanda. (2023): Ambient Noise Data Processing to Obtain Group Velocity for Subsurface Structure Identification: Preliminary Research in Hululais Geothermal Field, Sumatra, Indonesia. *Journal of Geoscience, Engineering, Environment, and Technology*, *8*(02–2), 67–71. https://doi.org/10.25299/jgeet.2023.8.02-2.13883

Fang, H., Yao, H., Zhang, H., Huang, Y. C., and Van Der Hilst, R. D. (2015): Direct inversion of surface wave dispersion for three-dimensional shallow crustal structure based on ray tracing: Methodology and application. *Geophysical Journal International*, *201*(3), 1251–1263. https://doi.org/10.1093/gji/ggv080

Fichtner, A. (2015): Source-structure trade-offs in ambient noise correlations. *Geophysical Journal International*, *202*(1), 678–694. https://doi.org/10.1093/gji/ggv182

Fukushima, S., Shinohara, M., Nishida, K., Takeo, A., Yamada, T., and Yomogida, K. (2024): Retrieval and precise phase-velocity estimation of Rayleigh waves by the spatial autocorrelation method between distributed acoustic sensing and seismometer data. *Geophysical Journal International*, *237*(2), 1174–1188. https://doi.org/10.1093/gji/ggae103

Gaucher, E., Toledo, T., Metz, M., Figueroa-Soto, A. G., and Calò, M. (2019): One year of passive seismic monitoring of the Los Humeros (Mexico) geothermal field. *European Geothermal Congress 2019*.

Gouédard, P., Yao, H., Ernst, F., and van der Hilst, R. D. (2012): Surface wave eikonal tomography in heterogeneous media using exploration data. *Geophysical Journal International*, *191*(2), 781–788. https://doi.org/10.1111/j.1365-246X.2012.05652.x

Granados-Chavarría, I., Calò, M., Figueroa-Soto, Á., and Jousset, P. (2022): Seismic imaging of the magmatic plumbing system and geothermal reservoir of the Los Humeros caldera (Mexico) using anisotropic shear wave models. *Journal of Volcanology and Geothermal Research*, *421*. https://doi.org/10.1016/j.jvolgeores.2021.107441

Guan, Z., and Niu, F. (2018): Using Fast Marching Eikonal Solver to Compute 3-D Pds Traveltime for Deep Receiver-Function Imaging. *Journal of Geophysical Research: Solid Earth*, *123*(10), 9049–9062. https://doi.org/10.1029/2018JB015892

Haerudin, N., Karyanto, and Kuntoro, Y. (2016): Radon and thoron mapping to delineate the local-fault in the way Ratai geothermal field lampung Indonesia. *ARPN Journal of Engineering and Applied Sciences*, *11*(7), 4804–4809.

Halim, I. S. A., Rambat, S., and Noh Muhammad, R. M. (2022): Site-Suitability Analysis on Seismic Stations using Geographic Information Systems. *Disaster Advances*, *15*(2), 1–14. https://doi.org/10.25303/1502da001014

Halliday, D., and Curtis, A. (2008): Seismic interferometry, surface waves and source distribution. *Geophysical Journal International*, *175*(3), 1067–1087. https://doi.org/10.1111/j.1365-246X.2008.03918.x

Ikeda, T., Tsuji, T., Konishi, C., and Saito, H. (2021): Spatial autocorrelation method for reliable measurements of two-station dispersion curves in heterogeneous ambient noise wavefields. *Geophysical Journal International*, *226*(2), 1130–1147. https://doi.org/10.1093/gji/ggab150

Irfan, R., and Daud, Y. (2019): Geothermal reservoir boundary delineation using 3D magnetotelluric inversion. case study: The 'delta' geothermal field of Indonesia. *IOP Conference Series: Earth and Environmental Science*, *254*(1), 1–12. https://doi.org/10.1088/1755-1315/254/1/012006

Janssen, M. T. G., Barnhoorn, A., Draganov, D., Wolf, K.-H. A. A., and Durucan, S. (2021): Seismic Velocity Characterisation of Geothermal Reservoir Rocks for CO2 Storage Performance Assessment. *Applied Sciences*, *11*(8), 3641. https://doi.org/10.3390/app11083641

Juliarka, B. R., and Iqbal, M. (2020): Model Gayaberat 2D Untuk Mengungkap Struktur Geologi Bawah Permukaan Pada Daerah Panas Bumi Natar. *Buletin Sumber Daya Geologi*, *15*(1), 39–49. https://doi.org/10.47599/bsdg.v15i1.292

Karyanto. (2003): Pencitraan Bawah Permukaan Daerah Panas Bumi Way Ratai Lampung Dengan Metode Tahanan Jenis 2 Dimensi. *Jurnal MIPA*, *9*(3), 55–59.

Karyanto, Haerudin, N., Mulyasari, R., Suharno, and Manurung, P. (2020): Geothermal Potential Assesment of Way Ratai Area Based on Thermal Conductivity Measurement to Measure Thermal Properties of Rocks. *Journal of the Earth and Space Physics*, *45*(4), 89–98. https://doi.org/10.22059/jesphys.2020.267095.1007048

Karyanto, Haerudin, N., Suharno, Darmawan, I., Adli, M., and Manurung, P. (2021): Numerical modeling for the steady-state condition of the geothermal system in Way Ratai. *Journal of Applied Science and Engineering*, *25*(3), 447–456. https://doi.org/https://doi.org/10.6180/jase.202206_25(3).0011

Karyanto, Prihantoro, R. H., and Darmawan, I. G. B. (2024a): Hydrothermal fluid flow permeability model simulation to identify potential zones for way Ratai geothermal reservoir. *AIP Conference Proceedings*, *2891*(1), 090004. https://doi.org/10.1063/5.0201529

Karyanto, Sihabudin, A., and Darmawan, I. G. B. (2022): Sensitivity test and enhancement of accelerometer instrument prototype capability in geothermal field. *AIP Conference Proceedings*, *2563*(1), 70002. https://doi.org/10.1063/5.0103246

Karyanto, Sihabudin, A., Darmawan, I. G. B., Suharno, and Manurung, P. (2024b): Characterising near-surface features of shallow shear wave velocity in the Way Ratai geothermal field. *Environmental Earth Sciences*, *83*(3), 90. https://doi.org/10.1007/s12665-023-11235-0

Larose, E., Carrière, S., Voisin, C., Bottelin, P., Baillet, L., Guéguen, P., Walter, F., Jongmans, D., Guillier, B., Garambois, S., Gimbert, F., and Massey, C. (2015): Environmental seismology: What can we learn on earth surface processes with ambient noise?. *Journal of Applied Geophysics, 116*, 62-74.. https://doi.org/10.1016/j.jappgeo.2015.02.001

Lehujeur, M., Le Chenadec, A., Vergne, J., Schmittbuhl, J., and EstOf-Team, the. (2016): Ambient seismic noise tomography using the dense array "EstOf" for deep geothermal exploration, Alsace, France. *European Geothermal Congress*.

Lehujeur, M., Vergne, J., Maggi, A., and Schmittbuhl, J. (2017): Ambient noise tomography with non-uniform noise sources and low aperture networks: Case study of deep geothermal reservoirs in northern Alsace, France. *Geophysical Journal International*, *208*(1), 193–210. https://doi.org/10.1093/gji/ggw373

Lehujeur, M., Vergne, J., Schmittbuhl, J., and Maggi, A. (2015): Characterisation of ambient seismic noise near a deep geothermal reservoir and implications for interferometric methods: a case study in northern Alsace, France. *Geothermal Energy*, *3*(3), 1–17. https://doi.org/10.1186/s40517-014-0020-2

Li, B., and Li, X. (2023): Study on the Test Error of Silt Dynamic Characteristic and Its Influence on the Peak Ground Acceleration. *HighTech and Innovation Journal*, *4*(1), 65–74. https://doi.org/10.28991/HIJ-2023-04-01-05

Li, X., Xu, Y., Xie, C., and Sun, S. (2022): Global characteristics of ambient seismic noise. *Journal of Seismology*, *26*(2), 343–358. https://doi.org/10.1007/s10950-021-10071-8

Liu, Y., Zhang, H., Fang, H., Yao, H., and Gao, J. (2018): Ambient noise tomography of three-dimensional near-surface shear-wave velocity structure around the hydraulic fracturing site using surface microseismic monitoring array. *Journal of Applied Geophysics*, *159*, 209–217. https://doi.org/10.1016/j.jappgeo.2018.08.009

Lynch, J. F., Wu, H. X., Pawlowicz, R., Worcester, P. F., Keenan, R. E., Graber, H. C., Johannessen, O. M., Wadhams, P., and Shuchman, R. A. (1993): Ambient noise measurements in the 200–300-Hz band from the Greenland Sea tomography experiment. *The Journal of the Acoustical Society of America*, *94*(2), 1015–1033. https://doi.org/10.1121/1.406949

Mangga, S. A., Amirudin, Suwarti, T., Gafoer, S., and Sidarto. (1993): *Geological Map of Tanjungkarang, Sumatra*. Bandung: Geological Research and Development Centre.

Martha, A. A., Cummins, P., Saygin, E., Sri Widiyantoro, and Masturyono. (2017): Imaging of upper crustal structure beneath East Java–Bali, Indonesia with ambient noise tomography. *Geoscience Letter*, *4*, 14. https://doi.org/10.1186/s40562-017-0080-9

Martins, J. E., Weemstra, C., Ruigrok, E., Verdel, A., Jousset, P., and Hersir, G. P. (2020): 3D S-wave velocity imaging of Reykjanes Peninsula high-enthalpy geothermal fields with ambient-noise tomography. *Journal of Volcanology and Geothermal Research*, *391*, 106685. https://doi.org/10.1016/j.jvolgeores.2019.106685

Matzel, E., Zeng, X., Thurber, C., Luo, Y., and Morency, C. (2017): Seismic Interferometry Using the Dense Array at the Brady Geothermal Field. *42nd Stanford Geothermal Workshop on Geothermal Reservoir Engineering*, *September*.

Meilinda, A., Adhani, A. T., Nurfaidah, H., Yogi, I. B. S., and Wibowo, R. C. (2023): Analisis Potensi Kerentanan Tanah Daerah Padang Cermin Menggunakan Metode Horizontal to Vertical Spectral Ratio. *Jurnal Lingkungan Dan Bencana Geologi*, *14*(2), 76–84.

Muksin, M., Bauer, K., Haberland, C., and Ryberg, T. (2013): Seismic imaging of the geothermal area in Tarutung (Sumatra, Indonesia): Comparison of local earthquake and ambient noise tomography. *Geophysical Research Abstracts EGU General Assembly*, *15*.

Nayak, A., Taira, T., Dreger, D. S., and Gritto, R. (2018): Empirical Green's tensor retrieved from ambient noise cross-correlations at The Geysers geothermal field, Northern California. *Geophysical Journal International*, *213*(1). https://doi.org/10.1093/gji/ggx534

Nishida, K. (2017): Ambient seismic wave field. *Proceedings of the Japan Academy, Series B*, *93*(7), 423–448. https://doi.org/10.2183/pjab.93.026

Nishida, K., Takagi, R., and Takeo, A. (2024): Ambient noise multimode surface wave tomography. *Progress in Earth and Planetary Science*, *11*(1), 4. https://doi.org/10.1186/s40645-023-00605-8

Patlan, E., Wamalwa, A., Kaip, G., and Velasco, A. A. (2013): Ambient noise cross-correlation study of Menengai caldera: Geothermal prospect in the Central Kenya Dome. *Transactions - Geothermal Resources Council*, *37*(PART 2).

Pranata, B., Yudistira, T., Widiyantoro, S., Brahmantyo, B., Cummins, P. R., Saygin, E., Zulfakriza, Z., Rosalia, S., and Cipta, A. (2020): Shear wave velocity structure beneath Bandung basin, West Java, Indonesia from ambient noise tomography. *Geophysical Journal International*, *220*(2). https://doi.org/10.1093/gji/ggz493

Rabinowitz, N., and Steinberg, D. M. (2000): *A Statistical Outlook on the Problem of Seismic Network Configuration* (pp. 51–69). https://doi.org/10.1007/978-94-015-9536-0_3

Rawlinson, N. (2005): FMST: Fast Marching Surface Tomography package–Instructions. In *Research School of Earth Sciences, Australian National University, Canberra.* Australian National University.

Rawlinson, N., Reading, A. M., and Kennett, B. L. N. (2006): Lithospheric structure of Tasmania from a novel form of teleseismic tomography. *Journal of Geophysical Research: Solid Earth*, *111*(2), 1–21. https://doi.org/10.1029/2005JB003803

Rawlinson, N., and Sambridge, M. (2004): Wave front evolution in strongly heterogeneous layered media using the fast marching method. *Geophysical Journal International*, *156*(3), 631–647. https://doi.org/10.1111/j.1365-246X.2004.02153.x

Rawlinson, N., and Sambridge, M. (2005): The fast marching method: An effective tool for tomographic imaging and tracking multiple phases in complex layered media. *Exploration Geophysics*, *36*(4), 341–350. https://doi.org/10.1071/EG05341

Ritzwoller, M. H., Lin, F. C., and Shen, W. (2011): Ambient noise tomography with a large seismic array. *Comptes Rendus - Geoscience*, *343*(8–9), 558–570. https://doi.org/10.1016/j.crte.2011.03.007

Rosalia, S., Cummins, P., Widiyantoro, S., Yudistira, T., Nugraha, A. D., and Hawkins, R. (2020): Group velocity maps using subspace and transdimensional inversions: Ambient noise tomography in the western part of Java, Indonesia. *Geophysical Journal International*, *220*(2), 1260–1274. https://doi.org/10.1093/gji/ggz498

Rosalia, S., Widiyantoro, S., Cummins, P. R., Yudistira, T., Nugraha, A. D., Zulfakriza, Z., and Setiawan, A. (2022): Upper crustal shear-wave velocity structure Beneath Western Java, Indonesia from seismic ambient noise tomography. *Geoscience Letters*, *9*(1). https://doi.org/10.1186/s40562-021-00208-5

Roth, E. G., Wiens, D. A., and Zhao, D. (2000): An empirical relationship between seismic attenuation and velocity anomalies in the upper mantle. *Geophysical Research Letters*,*27*(5),601–604.https://doi.org/10.1029/1999GL005418

Sánchez-Pastor, P., Obermann, A., Reinsch, T., Ágústsdóttir, T., Gunnarsson, G., Tómasdóttir, S., Hjörleifsdóttir, V., Hersir, G. P., Ágústsson, K., and Wiemer, S. (2021): Imaging high-temperature geothermal reservoirs with ambient seismic noise tomography, a case study of the Hengill geothermal field, SW Iceland. *Geothermics*, *96*, 102207. https://doi.org/10.1016/j.geothermics.2021.102207

Sarjan, A. F. N., Zulfakriza, Z., Nugraha, A. D., Rosalia, S., Wei, S., Widiyantoro, S., Cummins, P. R., Muzli, M., Sa-

hara, D. P., Puspito, N. T., Priyono, A., and Afif, H. (2021): Delineation of Upper Crustal Structure Beneath the Island of Lombok, Indonesia, Using Ambient Seismic Noise Tomography. *Frontiers in Earth Science*, *9*. https://doi.org/10.3389/feart.2021.560428

Sarkowi, M., Wibowo, R. C., and Karyanto. (2021): Geothermal Reservoir Identification in Way Ratai Area Based on Gravity Data Analysis. *Journal of Physics: Conference Series*, 012004. https://doi.org/10.1088/1742-6596/2110/1/012004

Saygin, E., and Kennett, B. L. N. (2012): Crustal structure of Australia from ambient seismic noise tomography. *Journal of Geophysical Research: Solid Eart*, *117*, B01304. https://doi.org/10.1029/2011JB008403

Seichter, S., Archodoulaki, V. M., Koch, T., Holzner, A., and Wondracek, A. (2017): Investigation of different influences on the fatigue behaviour of industrial rubbers. *Polymer Testing*, *59*, 99–106. https://doi.org/10.1016/j.polymertesting.2017.01.018

Sulandari, B., Suteja, A., Hadibroto, H., Nurmaliah, Setyanta, B., and Garniwa, A. (2023): Deliniasi Struktur Sesar Lampung-Panjang dan Identifikasi Potensi Sumberdaya Alam Berdasarkan Anomali Magnet Daerah Bandar Lampung. *Jurnal Geologi Dan Sumberdaya Mineral*, *24*(4), 195–203. https://doi.org/10.33332/jgsm.geologi.v24i4.721

Suryadi, Haerudin, N., Karyanto, and Sudrajat, Y. (2017): Identifikasi Struktur Bawah Permukaan Lapangan Panas Bumi Way Ratai Berdasarkan Data Audio Magnetotelluric (AMT). *Jurnal Geofisika Eksplorasi*, *3*(1), 85–97.

Takagi, R., Nishida, K., Maeda, T., and Obara, K. (2018): Ambient seismic noise wavefield in Japan characterised by polarisation analysis of Hi-net records. *Geophysical Journal International*, *215*(3), 1682–1699. https://doi.org/10.1093/gji/ggy334

Taufiq. (2020): Gravity Modelling and Second Vertical Derivative Calculation to Analysis Subsurface Structure at Wayratai Geothermal Prospect Area, Lampung. *IOP Conference Series: Materials Science and Engineering*, *982*(1). https://doi.org/10.1088/1757-899X/982/1/012049

Tian, Y., and Ritzwoller, M. H. (2017): Improving ambient noise cross-correlations in the noisy ocean bottom environment of the Juan de Fuca plate. *Geophysical Journal International*, *210*(3), 1787–1805. https://doi.org/10.1093/gji/ggx281

Trnkoczy, A., Bormann, P., Hanka, W., Holcomb, L. G., and Nigbor, R. L. (2009): Site Selection, Preparation and Installation of Seismic Stations. *Bormann, P.(Ur.)*, *1*(August), 1–108. http://gfzpublic.gfz-potsdam.de/pubman/item/escidoc:43206

Tryggvason, A., Rognvaldsson, S. T., and Flovenz, O. G. (2002): Three-dimensional imaging of the P- and S-wave velocity structure and earthquake locations beneath Southwest Iceland. *Geophysical Journal International*, *151*(3), 848–866. https://doi.org/10.1046/j.1365-246X.2002.01812.x

Uhrhammer, R. A. (1980): Analysis of small seismographic station networks. *Bulletin of the Seismological Society of America*, *70*(4), 1369–1379. https://doi.org/10.1785/BSSA0700041369

Utama, W., Indriani, R. F., Hermana, M., Anjasmara, I. M., Garini, S. A., and Putra, D. P. N. (2024): Towards Improving Sustainable Water Management in Geothermal Fields: SVM and RF Land Use Monitoring. *Journal of Human, Earth, and Future*, *5*(2), 216–242. https://doi.org/10.28991/HEF-2024-05-02-06

van Hal, V. H. J., Muller, J. W., van Sambeek, M. R. H. M., Lopata, R. G. P., and Schwab, H. M. (2023): An aberration correction approach for single and dual aperture ultrasound imaging of the abdomen. *Ultrasonics*, *131*. https://doi.org/10.1016/j.ultras.2023.106936

Verdel, A., Boullenger, B., Martins, J. E., Obermann, A., Toledo, T., and Jousset, P. (2019): Ambient noise seismic reflection interferometry at the Los Humeros geothermal field, Mexico. *European Geothermal Congress 2019*, 1–9.

Viens, L., Koketsu, K., Miyake, H., Sakai, S., and Nakagawa, S. (2016): Basin-scale Green's functions from the ambient seismic field recorded by MeSO-net stations. *Journal of Geophysical Research: Solid Earth*, *121*(4), 2507–2520. https://doi.org/10.1002/2016JB012796

Wahida, A., Wijaya, H., Yudistira, T., and Sule, M. R. (2018): Ambient noise tomography for geothermal exploration, a case study of WWs geothermal field. *AIP Conference Proceedings*, *1987*, 020101. https://doi.org/10.1063/1.5047386

Wang, J., Wu, G., and Chen, X. (2019): Frequency-Bessel Transform Method for Effective Imaging of Higher-Mode Rayleigh Dispersion Curves From Ambient Seismic Noise Data. *Journal of Geophysical Research: Solid Earth*, *124*(4), 3708–3723. https://doi.org/10.1029/2018JB016595

White, M. C. A., Fang, H., Nakata, N., and Ben-Zion, Y. (2020): PyKonal: A python package for solving the eikonal equation in spherical and cartesian coordinates using the fast marching method. *Seismological Research Letters*, *91*(4), 2378–2389. https://doi.org/10.1785/0220190318

Widiatama, A. J., Hendrawan, R. N., Ogara, E. R., Santy, L. D., Evitayanti, V. I., and Sagala, L. S. N. (2022): Formasi Sabu Sebagai Endapan Kolisi Busur Gunungapi Woyla dengan Lempeng Sumatra Barat. *Jurnal Geosains Dan Teknologi*, *5*(2), 104–115. https://doi.org/10.14710/jgt.5.2.2022.104-115

Wu, Q., Mi, H. Z., Li, Y. B., and Li, Y. G. (2022): Study on the Improved Method for Calculating Traveltime and Raypath of Multistage Fast Marching Method. *Minerals*, *12*(12), 1624. https://doi.org/10.3390/min12121624

Xia, S., Zhang, C., and Cao, J. (2023): Ambient Noise Tomography for Coral Islands. *Engineering*, *25*, 182–193. https://doi.org/10.1016/j.eng.2021.09.022

Xu, W., Ding, Z., Wu, P., Lu, L., and Qin, T. (2023): Improved 3D Shallow-Deep Vs Structure in Tongzhou, Beijing (China), Revealed by Dense Array Ambient Noise Tomography. *Earth and Space Science*, *10*(5). https://doi.org/10.1029/2022EA002707

Yang, X., Bryan, J., Okubo, K., Jiang, C., Clements, T., and Denolle, M. A. (2023): Optimal stacking of noise cross-correlation functions. *Geophysical Journal International*, *232*(3). https://doi.org/10.1093/gji/ggac410

Yang, Y., and Ritzwoller, M. H. (2008): Characteristics of ambient seismic noise as a source for surface wave tomogra-

phy. *Geochemistry, Geophysics, Geosystems*, *9*(2). https://doi.org/10.1029/2007GC001814

Yao, H. (2015): *Manual for EGF Analysis Time Freq Dispersion Software*. University of Science and Technology of China.

Yao, H., Beghein, C., and Van Der Hilst, R. D. (2008): Surface wave array tomography in SE Tibet from ambient seismic noise and two-station analysis - II. Crustal and upper-mantle structure. *Geophysical Journal International*, *173*(1). https://doi.org/10.1111/j.1365-246X.2007.03696.x

Yao, H., Gouédard, P., Collins, J. A., McGuire, J. J., and van der Hilst, R. D. (2011): Structure of young East Pacific Rise lithosphere from ambient noise correlation analysis of fundamental- and higher-mode Scholte-Rayleigh waves. *Comptes Rendus - Geoscience*, *343*(8–9). https://doi.org/10.1016/j.crte.2011.04.004

Yao, H., and van der Hilst, R. D. (2009): Analysis of ambient noise energy distribution and phase velocity bias in ambient noise tomography, with application to SE Tibet. *Geophysical Journal International*, *179*(2). https://doi.org/10.1111/j.1365-246X.2009.04329.x

Yao, H., van der Hilst, R. D., and de Hoop, M. V. (2006): Surface-wave array tomography in SE Tibet from ambient seismic noise and two-station analysis - I. Phase velocity maps. *Geophysical Journal International*, *166*(2). https://doi.org/10.1111/j.1365-246X.2006.03028.x

Zhou, C., Xia, J., Pang, J., Cheng, F., Chen, X., Xi, C., Zhang, H., Liu, Y., Ning, L., Dai, T., Mi, B., and Zhou, C. (2021): Near-Surface Geothermal Reservoir Imaging based on the Customised Dense Seismic Network. In *Surveys in Geophysics* (Vol. 42, Issue 3). https://doi.org/10.1007/s10712-021-09642-8

Zulfakriza, Z., Nugraha, A. D., Widiyantoro, S., Cummins, P. R., Sahara, D. P., Rosalia, S., Priyono, A., Kasbani, K., Syahbana, D. K., Priambodo, I. C., Martanto, M., Ardianto, A., Husni, Y. M., Lesmana, A., Kusumawati, D., and Prabowo, B. S. (2020): Tomographic Imaging of the Agung-Batur Volcano Complex, Bali, Indonesia, From the Ambient Seismic Noise Field. *Frontiers in Earth Science*, *8*. https://doi.org/10.3389/feart.2020.00043

Zulfakriza, Z., Saygin, E., Cummins, P. R., Widiyantoro, S., Nugraha, A. D., Lühr, B. G., and Bodin, T. (2014): Upper crustal structure of central Java, Indonesia, from transdimensional seismic ambient noise tomography. *Geophysical Journal International*, *197*(1). https://doi.org/10.1093/gji/ggu016

SAŽETAK

Mapiranje Rayleighevih valnih grupa iz ambijentalnoga šuma u geotermalnome polju Way Ratai pomoću prototipova seizmografa PiGraf

Od 2018. istraživački tim istražuje i razvija prototip senzora za bilježenje seizmičke aktivnosti. Nadogradnja je razvijena i mora se potvrditi, ponajprije za praćenje aktivnosti ambijentalnoga šuma u geotermalnome okruženju. Cilj je ove studije odrediti grupnu brzinu Rayleighevih valova korištenjem analize tomografije ambijentalnoga šuma (ANT) u geotermalnoj regiji Way Ratai primjenjujući četiri PiGraf prototipa seizmografa. Metoda prikupljanja podataka jest postavljanje stacionarne međustanice udaljene oko 5 kilometara (km) sedam uzastopnih dana, sa 100 uzoraka u sekundi (SPS). Brza površinska tomografija (FMST) korištena je za generiranje grupne brzine iz poprečno koreliranih vremenskih nizova, što proizvodi tomografske slike. Rezultati su pokazali da distribucija energije ambijentalnoga šuma potječe od sjeverozapada prema jugoistoku, najvjerojatnije s mora. U isto vrijeme grupna brzina iz Greenove funkcionalne skupine u rasponu perioda od 0,2 s do 0,5 s, 0,5 s do 1 s i 1 s do 5 s iznosi redom 0,337 km/s, 0,415 km/s i 0,427 km/s. Ove su vrijednosti usklađene unutar raspona brzina disperzijske krivulje od 0,3 do 0,8 km/s. Modeliranje grupne brzine Rayleighevih valova u rasponu perioda od 0,5 s do 1 s također je identificiralo obrazac koji odgovara geotermalnom potencijalnom području potvrđujući prethodne nalaze. Međutim, jasnoća poprečnoga korelograma Greenove funkcionalne skupine identificirana je kao tema za daljnje istraživanje s više postaja i duljim vremenima mjerenja.

Ključne riječi:
tomografija ambijentalnoga šuma, geotermalnost, PiGraf prototip, grupna brzina Rayleighevih valova, Way Ratai

Author's contribution

Karyanto (1) (Dr., Lecturer, Geophysics) provided the ambient noise analysis, Rayleigh wave group velocities interpretations and the presentation of the results. **Haidar Prida Mazzaluna (2)** (Student, Geophysics) performed the fieldwork, contributing to the ambient noise data acquisition. **I Gede Boy Darmawan (3)** (Lecturer, Geophysics) provided the PiGraf prototype system preparation and calibration. **Rahmat Catur Wibowo (4)** (Lecturer, Geophysics) performed the fieldwork, contributing to the geology of the Way Ratai geothermal field. **Ahmad Zaenudin (5)** (Dr., Lecturer, Geophysics) performed the fieldwork, contributing to the PiGraf acquisition station and monitoring. **Maman Hermana (6)** (Dr., Lecturer, Geosciences) provided the group velocity of dispersion curve analysis.